



Process-Geometry Interplay in the Deposition and Microstructural Evolution of 7YSZ Thermal Barrier Coatings by Air Plasma Spray

Edward J. Gildersleeve V¹ · Sanjay Sampath¹

Submitted: 14 January 2020 / in revised form: 25 February 2020 / Published online: 13 March 2020
© ASM International 2020

Abstract Air plasma spray (APS) yttria-stabilized zirconia (7YSZ) TBCs are often deposited onto model planar surfaces for microstructural evaluation and testing. Recently, an interest on the implications of both TBC deposition and performance on more complex geometries has developed in the scientific and industrial community, as the microstructures can be substantially different depending on the substrate geometry with concomitant implications on performance (e.g. leading-edge failure). In this study, the implications of processing TBCs on cylindrical substrates as opposed to planar surfaces are explored. Particle diagnostics were conducted to understand differences in coating formation dynamics between planar and cylindrical targets. Scanning Electron Microscopy and Image Analysis were concurrently used to quantitatively define the porosity differences among multiple conditions of spraying and to benchmark the transition of porosity from disk to cylinder. Additionally, rods of different radii of curvature were explored in this study to evaluate the effect of the radius of curvature on the TBC deposit microstructure. Finally, a modified approach to established thermoelastic beam curvature techniques is introduced which can see subtle changes in the mechanical properties of coatings produced at torch traverse conditions similar to how they are produced on a curved surface.

Keywords 7YSZ · Air plasma spray · curved surface spraying · Thermal barrier coating

Introduction

Thermal barrier coatings (TBCs) based on 7-wt.% yttria-stabilized zirconia (7YSZ) are widely used in the power generation and aircraft industry which act primarily to protect the underlying metal substrate from incident high heat flux. There are two primarily dominant deposition technologies in the industry for producing TBCs: electron beam physical vapor deposition (EB-PVD) and air plasma spray (APS) (Ref 1, 2). Both processes come with their advantages and disadvantages, which are exacerbated when considering parts which have complex geometries. In the case of EB-PVD, the incident vapor cloud and its interactions with the substrate govern the microstructural development. As such, EB-PVD is a unique process as the vapor cloud of coating material which engulfs the substrate is capable of producing a highly uniform coating microstructure and thickness at all points along a surface (Ref 3, 4). Notwithstanding this, Liu et al. (Ref 5) showed when considering a turbine blade-type geometry, the microstructure and residual stress states of the 7YSZ EB-PVD coatings as well as the thickness distribution can change in a significant way depending on the sharpness of the curvature to which the vapor cloud is incident. Likewise, Hass et al. (Ref 6) reported the sensitivity of EB-PVD microstructures on the angle of the incident vapor cloud with respect to the target surface. Similar findings have been reported throughout the literature which suggests the sensitivity of substrate curvature on TBC property (Ref 7–9).

Unlike EB-PVD, APS as a line-of-sight deposition process is much more sensitive to changes in surface topography and geometry. In APS, the rapid solidification of the feedstock droplets into “splats” has been shown to be the primary building block to the coating microstructure

✉ Sanjay Sampath
sanjay.sampath@stonybrook.edu

Edward J. Gildersleeve V
edward.gildersleeve@stonybrook.edu

¹ Center for Thermal Spray Research, Stony Brook, NY 11794-2275, USA

(Ref 10–14). Furthermore, it has been shown that due to the line-of-sight nature of the process, the angle at which these droplets impact the surface can also have implications on the coating microstructure and overall mechanical and thermal properties (Ref 15). Liu et al. (Ref 16) specifically demonstrates the effect of multiple curvatures on a given substrate on the resulting microstructure as well as the residual stresses and failure modes of an APS 7YSZ TBC on a turbine blade-type geometry. Likewise it has been shown by Lance et al. (Ref 17) when comparing simply flat versus curved substrates demonstrating the dramatic change in TBC durability with the change in substrate curvature. From these works, the influence part geometry can have on the end-result after deposition is quite evident. Additionally, it has been corroborated elsewhere in the literature that the radius of curvature of a substrate can more sensitively impact the residual stress state of the coating as well as the delamination mechanics of the film in service; this can be attributed to the intrinsic changes in the microstructure while depositing APS coatings on substrates with curvature (Ref 8, 18, 19).

This study strives to bridge the gap between qualitative microstructural analysis of coatings on different substrate geometries and quantitative property measurements. The microstructural implications when depositing 7YSZ TBCs by APS on model planar disk surfaces versus cylindrical geometries are compared as a first-order analysis. Figure 1 illustrates a schematic which shows experimental observations of how rods of a small enough radius of curvature have the propensity to “cut” the plasma-particle plume. Depending on the centering of the torch face to the vertical axis of the part, certain portions of the plume can be preferentially selected. Unlike how rods were coated in this study, when spraying a disk, a “ladder-type” spray raster pattern was used to uniformly overlay the surface with the same deposit microstructure. The vertical “step size” of the ladder pattern is typically governed by the microstructural changes along the pseudo-gaussian distribution of the deposit.

To characterize the influences substrate curvature may have on the resulting coating microstructure, the particle diagnostic system DPV-2000 was used to generate 2-D plume maps of the particle state. This was done in

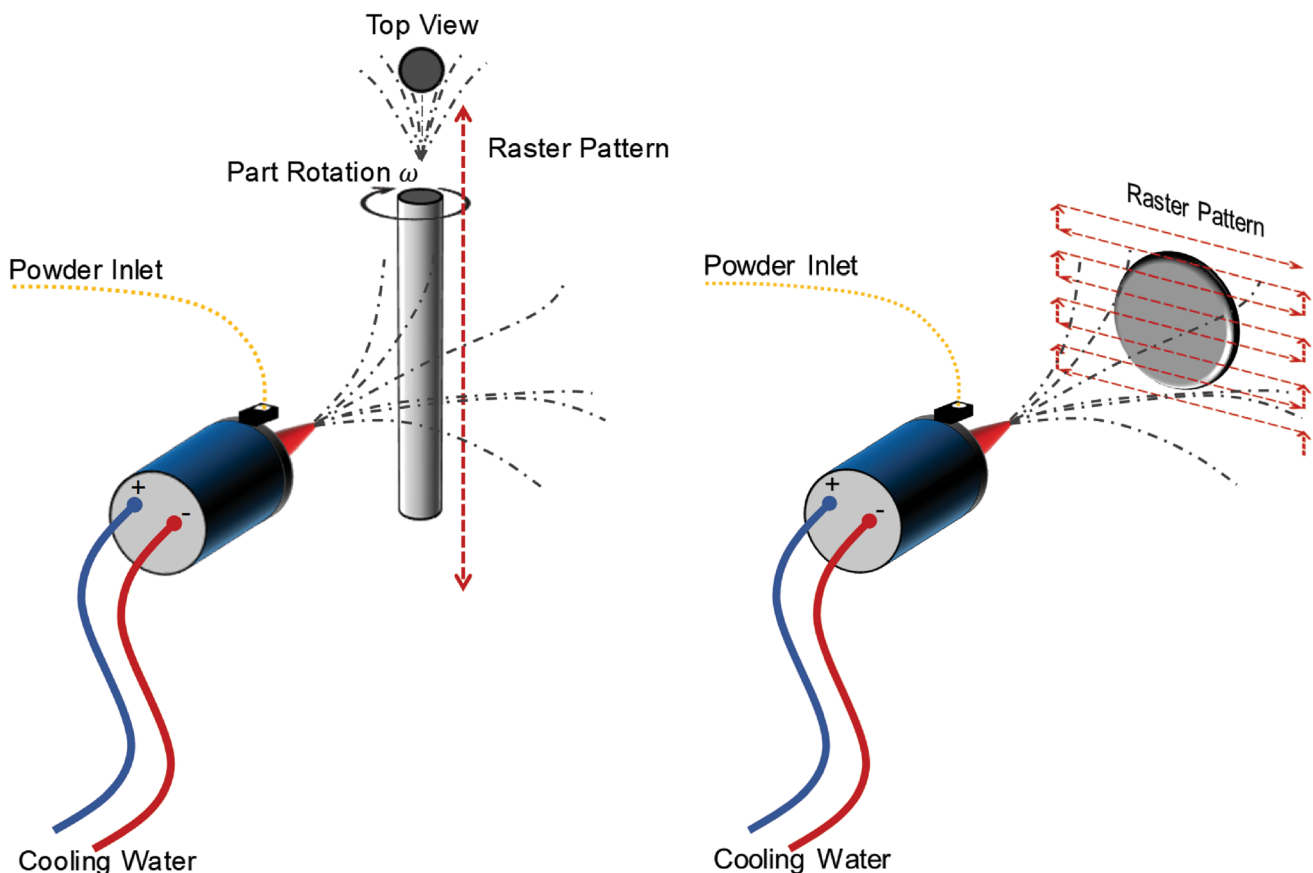


Fig. 1 Schematic illustrating the deposition patterns for rod and disk samples

conjunction with cross-sectional microstructural analysis using scanning electron microscopy. Due to the subtle nature of the differences in microstructure which are difficult to ascertain through the above methods, a thermoelastic beam curvature technique was employed to evaluate the nonlinear elastic mechanical properties of coatings sprayed by “cutting” the plume in different preferential positions (Ref 20, 21). Attempts to draw correlations between these microstructural features and the property measurements were carried out.

The work presented here intends to illustrate the differences between flat and curved substrate coupons or parts in the context of thermal barrier coating deposition, microstructure, and property. To do so, inflight particle properties are characterized in multiple dimensions to provide insights on the spatial distribution of the molten/semimolten droplets. Additionally, metallography and image analysis are utilized to highlight subtle differences in the as-deposited microstructure of these coatings. Through image analysis, an understanding of the subtle differences in the 2-D structure is established. From this first-principles approach, further characterization of the mechanical properties of these coatings was conducted. Modified substrate geometries compatible with previously established curvature techniques were introduced to enable this characterization. From these modified substrates, insights into the nonlinear elastic properties of the coatings were ascertained. These properties were reconciled with what is observed microstructurally to provide insights into the formation dynamics of plasma-sprayed thermal barrier coatings for substrates of complex geometry. From these data, conclusions can be drawn about the influence of

substrate (coupon or part) geometry on the microstructure and property of the final deposited coating.

Experimental

7YSZ coatings were sprayed onto both flat and cylindrical Mar-M 247 substrates using either an F4-MB gun (Oerlikon Metco, Westbury, NY) controlled by a Plasma-Tech A3000 Plasma Control System or a Sinplex-Pro™ Cascaded Plasma Torch controlled by a 9MC Plasma Control Unit (Oerlikon Metco, Westbury, NY). The powder used was Hollow Spherodized (HOSP) powder of either an ensemble particle size distribution (nominally 10–105 μm in size) or a finer cut (nominally 10–45 μm in size) (SG204/204F, Saint-Gobain, Worcester, MA), and further details can be found elsewhere (Ref 22). The deposition procedure for spraying onto cylindrical substrates is outlined schematically in Fig. 2. A mask with several 25.4-mm-wide “windows” was placed in front of the continuously rotating specimen to allow for the production of multiple samples on one substrate in one deposition run. These samples were then machined free into “rodlets.” The plasma gas flow rates, arc current, etc., are outlined in Table 1.

Once freed, these rodlets were mounted in two-part epoxy (Buehler Epothin2, Buehler Inc., Lake Bluff, IL) with vacuum impregnation to strengthen the coating against machining cracks. As a full mount, the rods were then cross-sectioned across the center with a high-speed diamond saw (Isomet 1000, Buehler Inc., Lake Bluff, IL) and polished to a $< 0.5 \mu\text{m}$ finish using standard

Fig. 2 Experimental setup used for spraying TBCs onto rods. Long rods are sprayed and subsequently sectioned into “rodlets”

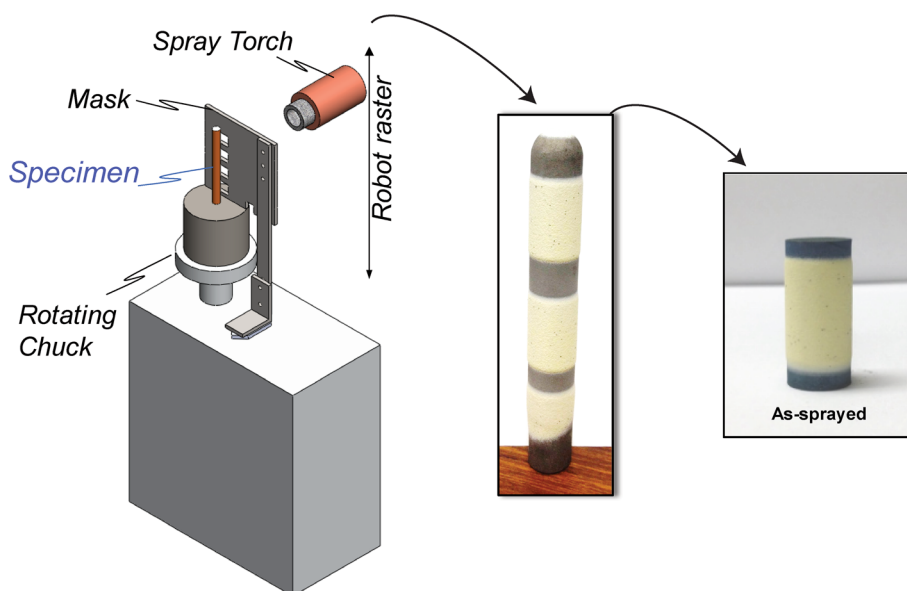


Table 1 Plasma conditions used to deposit 7YSZ coatings

Condition	Plasma torch	Ar, slpm	H ₂ , slpm	Current, A	Power, Kw	Powder	Standoff distance, mm	Surface speed, mm/s
C1	Conventional	47.5	6	550	34	Ensemble	150	500
C2	Conventional	47.5	6	550	34	Ensemble	150	157
C3	Conventional	47.5	6	550	34	Ensemble	200	157
C4	Conventional	47.5	6	550	34	Fine	200	157
C5	Cascaded	47.5	6	550	49	Ensemble	200	157

metallographic procedures. The mounting and polishing procedure of all samples in this work reflects the methods described above.

Sample microstructures were viewed using scanning electron microscopy with a Hitachi TM-3000 tabletop scanning electron microscope in the backscatter mode. For porosity analysis, ten images at a set magnification were taken, adjusted for optimal brightness and contrast, and then analyzed in a MATLAB program which uses algorithms adapted from Leigh et al. to evaluate the total 2D-porosity of the coating while also quantifying the presence of interlamellar porosity, globular pores, and microcrack content within the coatings (Ref 23).

Characterization of the spray process was carried out through use of the DPV-2000 (Tecnar Inc., QA, Canada) (Ref 24, 25). Measurements of the particle state were taken in two modes: at the center of maximum counted particles within the plume and as a 30 mm × 30 mm grid with a step size of 1 mm and measurement time of 3 s per data point. Estimation of the particle melting temperature was done through analysis techniques described by Vasudevan et al. (Ref 26) and were conjunctively used with the grid scans to illustrate the spatial distribution of molten particles in the plume at a given standoff distance.

To quantify the mechanical properties of some of the coatings, thermoelastic beam curvature techniques established in prior works were used to estimate the coating modulus. While achieving exactly similar coatings on a cylinder and a beam surface is incredibly challenging, a flat substrate geometry was designed to simulate the experimentally observed plume “cutting” when spraying sharp edges/curved surfaces. To do this, a 228.6 × 25.4 mm rectangular plate was machined into the shape of an I-beam with a gauge width of 7.94 mm. This I-beam shape is unique in that it allows for spraying the surface without the use of a ladder-type spray pattern (as would be the case for buttons or full-sized plates). Thus, it is possible to selectively sample a smaller percentage of the plasma plume than the full 25.4-mm-wide space. After spraying was complete, the I-beam was removed from the booth and placed in a furnace equipped with laser displacement sensors to carry out *ex situ* isothermal beam curvature

measurements. Here, techniques by Liu et al. (Ref 20, 21) were employed to convert the curvature/temperature measurements into stress/strain data. Inverse analysis was used to compute the degree of nonlinearity in the coatings sprayed on I-beams.

Results and Discussion

The results presented below seek to provide a framework of experimental data to assist in conceptualizing and understanding the influence of substrate geometry on the plasma plume/particle/part interactions. Careful microstructural investigations in conjunction with strategic deposition strategies on modified substrates have allowed for collaborative analysis of the influence of the part geometry on the microstructure as well as the resulting mechanical properties of the as-deposited coatings. In the following discussion, it will be shown while the microstructural differences are subtle, these differences can be more easily seen through employing advanced characterization techniques.

Preliminary Microstructural Investigations

As a preliminary analysis, coatings were sprayed on disks and rods, while attempting to match as many parameters as possible (plasma condition, feed rate, surface speed, etc.). Figure 3 shows the as-deposited microstructures of a 7YSZ TBC deposited on a 25.4-mm \emptyset flat button (Sample A1) and 12.5-mm \emptyset rod (Sample A2). Differences in overall porosity can be observed (see Table 2), which was confirmed by measurement of elastic modulus by micro-indentation on the cross section through methods published by Oliver and Pharr (Ref 27).

Figure 4 shows the longitudinal cross section of a 7YSZ deposit at 200-mm standoff distance using plasma condition C3. It is important to note the dimensional length of this plume profile is nearly 25.4 mm. This length implies that the masking technique shown in Fig. 2 allows for approximately the entirety of the plasma plume to pass through its machined windows with minimal obstruction or

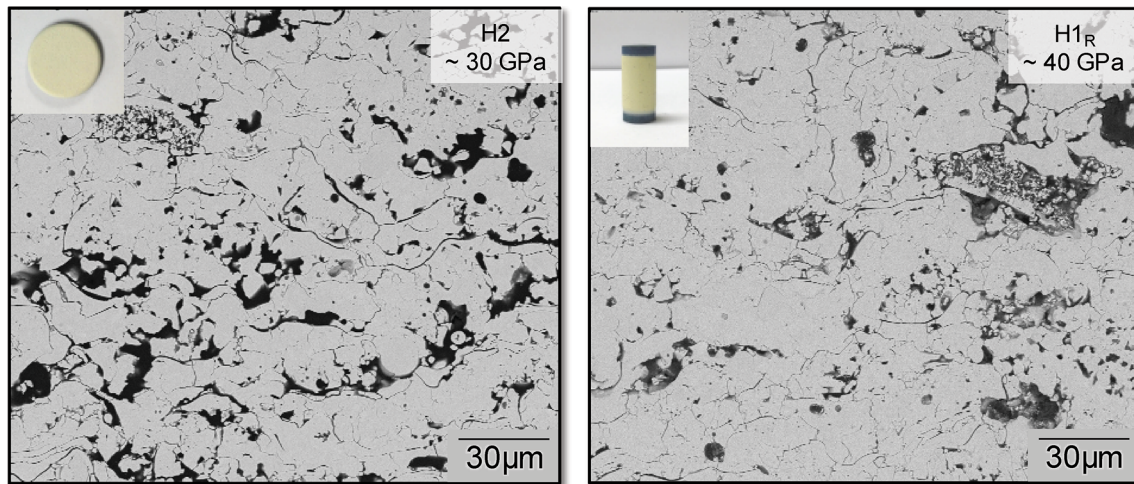


Fig. 3 Microstructures of 7YSZ TBCs sprayed on a flat button (Sample A1) and rod (Sample A2) for equivalent spraying conditions. Elastic modulus measurements by micro-indentation are also included

Table 2 Measured porosity by image analysis using methods proposed by Leigh et al. for all samples considered in this study

Condition	Sample ID	Substrate type	Interlamellar porosity, %	Globular porosity, %	Microcrack content, %	Total porosity, %
C1	A1	25.4-mm \emptyset button	1.5 ± 0.2	12.4 ± 1.4	6.9 ± 0.4	20.8 ± 1.2
C2	A2	12.5-mm $\sim \emptyset$ rod	0.6 ± 0.2	10.4 ± 0.9	6.1 ± 0.7	17.1 ± 0.5
C3	A3	12.5-mm $\sim \emptyset$ rod	2.1 ± 0.5	7.1 ± 1.2	11.2 ± 0.9	20.4 ± 1.4
C3	A4	25.4-mm $\sim \emptyset$ rod	2.8 ± 0.9	8.7 ± 1.4	12.9 ± 1.1	24.4 ± 1.6
C3	A5	Full-width beam	4.3 ± 1.0	9.9 ± 1.4	13.7 ± 0.9	28.0 ± 1.8
C3	A6	Thin-gauge beam	3.1 ± 0.6	11.5 ± 1.4	9.7 ± 0.9	24.4 ± 1.4
C4	A7	12.5-mm $\sim \emptyset$ rod	0.8 ± 0.3	11.4 ± 1.4	8.3 ± 0.6	20.4 ± 0.4
C4	A8	25.4-mm $\sim \emptyset$ rod	1.6 ± 0.1	7.9 ± 1.3	13.1 ± 1.5	22.4 ± 0.4
C5	A9	12.5-mm $\sim \emptyset$ rod	0.8 ± 0.2	5.1 ± 1.2	8.0 ± 0.5	13.8 ± 1.1
C5	A10	25.4-mm $\sim \emptyset$ rod	0.7 ± 0.2	5.9 ± 1.0	7.9 ± 0.5	14.6 ± 0.7

interaction. In Fig. 4, it can also be seen that in addition to the difference in thickness across the length, there are characteristic differences in the bonding between splats at the left/right and center of this profile. Comparing Fig. 4(c) versus Fig. 4(d) shows the distance between constituent splats overall is quite different when comparing images taken at the same magnification. In some cases, the distance between splat boundaries was measured to be 100% greater in the left/right periphery of the plume deposit than in the axial center. This is suggestive of a significant spatial gradient in particle state of the plasma plume. Additionally from the figure, it can be argued qualitatively that the resulting porosity of the left/right periphery is higher than that of the axial center. Furthermore, when spraying a pin as shown in Fig. 2, if the rod is centered to the plume (see Fig. 1), it is clear the majority of sampling during spray would be of particles which created the microstructure in the center of this profile, which would

consequently produce a denser microstructure. Similar conclusions were drawn from modeling studies by multiple authors in the field of modeling thermal spray processes. Kang and Ba performed extensive modeling studies to determine the influence the presence of a substrate/part with different curvatures might have on the incoming plasma plume (Ref 28, 29). Of note in their findings is the following: substrate curvature heavily influences the gas velocities and jet temperatures exiting a plasma torch. Additionally, from these studies, it was determined for a given set of deposition conditions (plasma gas combinations, arc current, feedstock, part geometry, etc.), there is a threshold particle size above which they are unsusceptible to the changes in gas flow. For curved surfaces, Ba illustrated both temperature and velocity of the plasma can decrease substantially from the axial center at locations on the periphery of the part. This undoubtedly can influence the resulting particle state at these locations. This effect

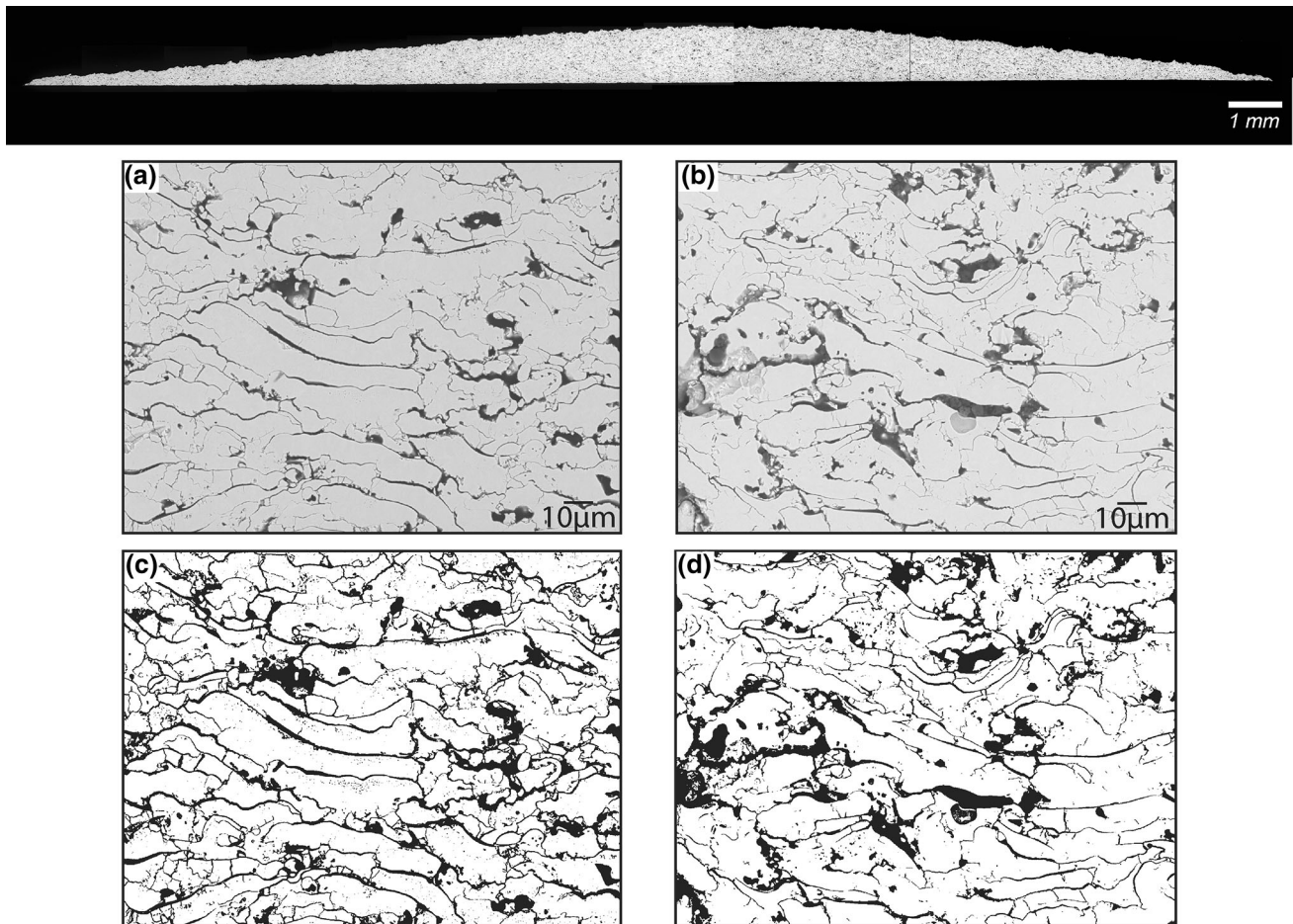


Fig. 4 Longitudinal cross-section microstructure of the plasma profile using ensemble 7YSZ powder. (a) The left periphery of the profile, (b) the center of the profile. (c, d) show binary thresholded images to illustrate the characteristic porosity of (a, b), respectively

was observed by both Kang and Ba to be less aggressive for flat parts. Likewise, Pourang (Ref 30), albeit for Suspension Plasma Spraying, deduced the propensity for deposition of a droplet was seen to be dependent on its size and incident momentum. This information serves as the basis toward a qualitative explanation of the inevitable denser as-deposited TBC microstructure a given condition would produce on a cylinder versus a flat coupon/plate.

Quantifying what is shown in Fig. 3 and 4 can be done through use of the DPV-2000 in the grid measurement mode. In this mode, the scanning head of the DPV-2000 moves in discrete increments as set by the user in 2 dimensions, taking particle data at each incremental point. Figure 5 shows the resulting spatial map of the temperature and particle flux from such a measurement at plasma condition C3. These 2-dimensional surface maps are centered about the location where the equipment counts a maximum number of particles passing through its measurement space. It is clear from the figure that along the horizontal *X*-direction, there is significant fluctuation in the

particle temperature with respect to the approximated melting temperature of the feedstock based on previously established techniques (Ref 31). Moreover, there is a distinct region of the profile which (specifically at the left periphery of the plume in this data) registers particle temperatures below this approximate melting temperature. Comparing the particle state at the plume periphery with the profile from Fig. 4, it can be seen at the left periphery, particles with temperatures at or below the melting point exist (hence the presence of unmelted/resolidified particles). Thus, with the deposition of nominally colder particles, a more porous microstructure is expected. It can be surmised the spatial distribution of the particle state would strongly influence the as-deposited TBC microstructure on the outer diameter of a cylindrical part and knowing the degree of the spatial distribution would assist in process optimization.

From this, a comparison between data presented in Fig. 5 with that shown in Fig. 4 can be executed. For instance, the *X*-line profile of Fig. 5(b) is essentially in the same plane as the microstructural view of Fig. 4. As such,

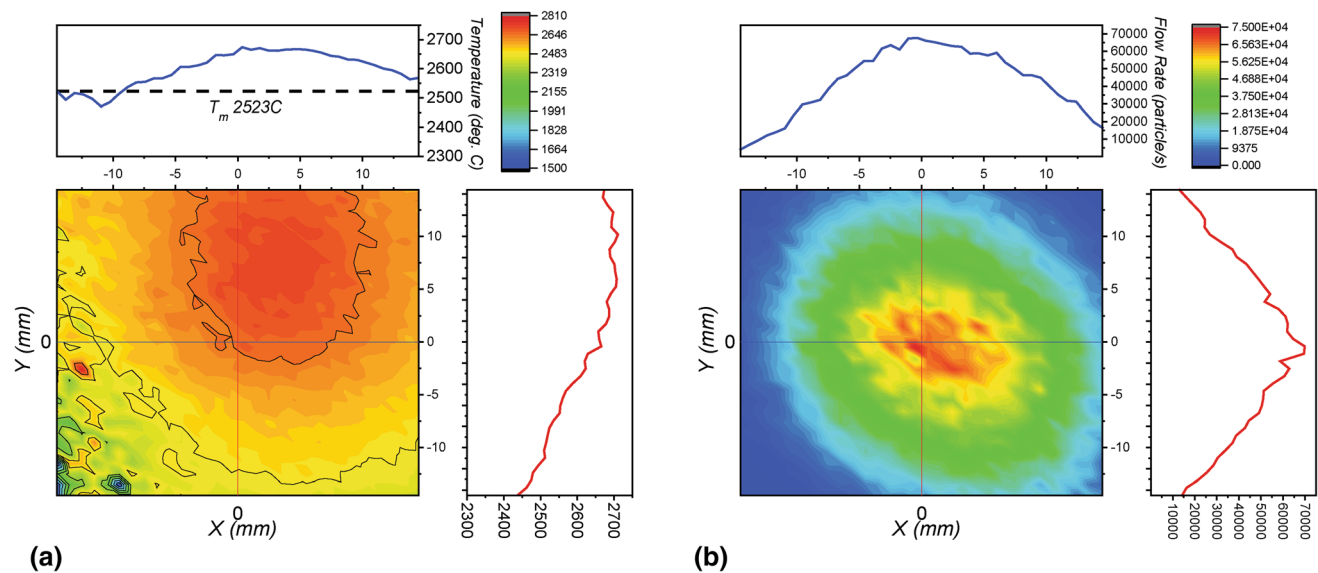


Fig. 5 (a) Thermal mapping in space of the particle temperatures for plasma condition C1. The particle melting temperature is overlaid on the longitudinal plot to illustrate the variation in temperature from

the pseudo-Gaussian shape of the data in Fig. 5(b) is similar to the shape of the coating deposit in Fig. 4. Beyond the thickness and shape of the deposit, the particle state data at the plume periphery suggests there should be a higher percentage of unmelted/resolidified particles trapped in the microstructure. Likewise, the splats which are present in the polished cross section from the same region have significantly higher boundary spacing. Previous studies have suggested the influence of substrate/surface temperature effects on the formation and bonding of yttria-stabilized zirconia splats on top of one another (Ref 32, 33). Based on these studies, it can be expected the presence of lower temperature droplets on the peripheries of the plume influenced the distance between resulting splats in the microstructure of Fig. 4 by reducing the temperature of the deposit surface. This methodology of spatial plume property characterization in conjunction with the analysis of the porosity and the mechanical properties of the coatings presented here will serve as the crux of the analysis toward how part geometry influences the resulting microstructure and property of air plasma-sprayed TBCs.

Influence of Plasma Torch Type on Plasma/Particle/Part Interactions

To further illustrate the influence of the spatial distribution of particle state in the plasma plume on TBC microstructure, a 25.4-mm \emptyset rod was sprayed using the same C3 condition (Sample A4) to compare against the 12.5-mm \emptyset rod (Sample A3). The resulting as-deposited microstructures of the two samples can be seen in Fig. 6. Here, again,

left-to-right. (b) Particle flow map in space for the C1 condition. The maximum particle flux (aka the center of the plasma plume) is in the center of the measurement space

we see that with the increase in part diameter, the porosity of the TBC increases. This is because now rather than sampling only the center of the plume with the highest degree of melt content, the 25.4-mm \emptyset rod is prone to sample the plume peripheries (as in the case of the button), and thus the porosity is driven to increase by roughly 4% as shown in Table 2.

The discrepancies in porosity which are generated by simply changing the size of the radius of curvature of the part brought about the fundamental question—can the plasma spray process be manipulated to develop consistently uniform microstructures for surfaces of different radii of curvature? One possible route for achieving such a microstructure is through use of a plasma torch with a more uniform thermal emission field. This is typically achieved with the technology of cascaded plasma torches. For this study, the Sinplex-ProTM was fitted with an 8-mm nozzle, similar to the F4-MB, using the same gas flow rates, arc current, and standoff. At these conditions, the 2D plume-particle state was again measured. The data in Fig. 7 do indeed confirm that with a torch that has a more uniform thermal field such as the Sinplex, the particle temperature spatial distribution has a less significant variance. Similar results were reported by Seshadri et al. (Ref 34) in comparing the point of feed rate saturation between the Sinplex-ProTM and F4-MB. Additionally, for equivalent conditions, the cascaded plasma torch seems to deliver more energy to the feedstock particles, which consequentially results in higher measured particle temperatures. These two observations conjunctively suggest the microstructures of cylinders with different radii of

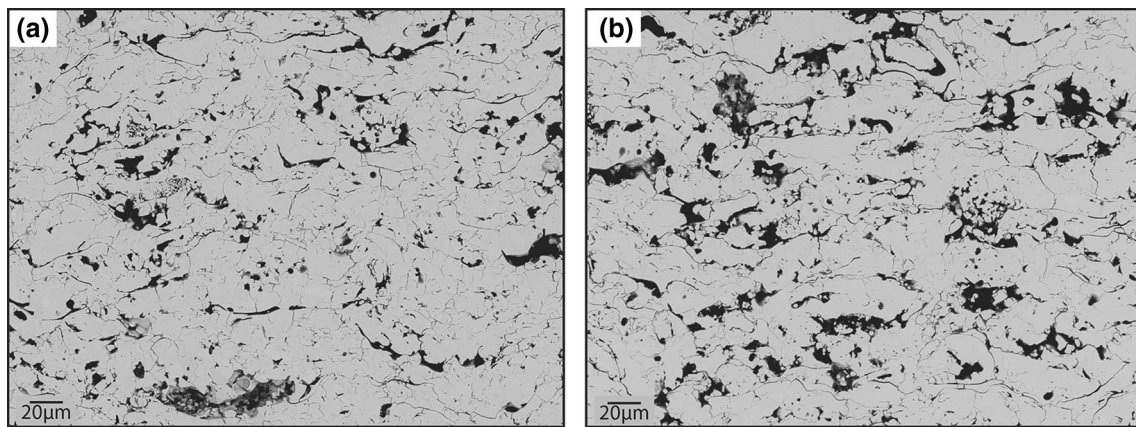


Fig. 6 As-deposited microstructures of 7YSZ TBCs for (a) 12.5-mm \emptyset rods (Sample A3) and (b) 25.4-mm \emptyset rods (Sample A4) for the same plasma condition and powder size distribution

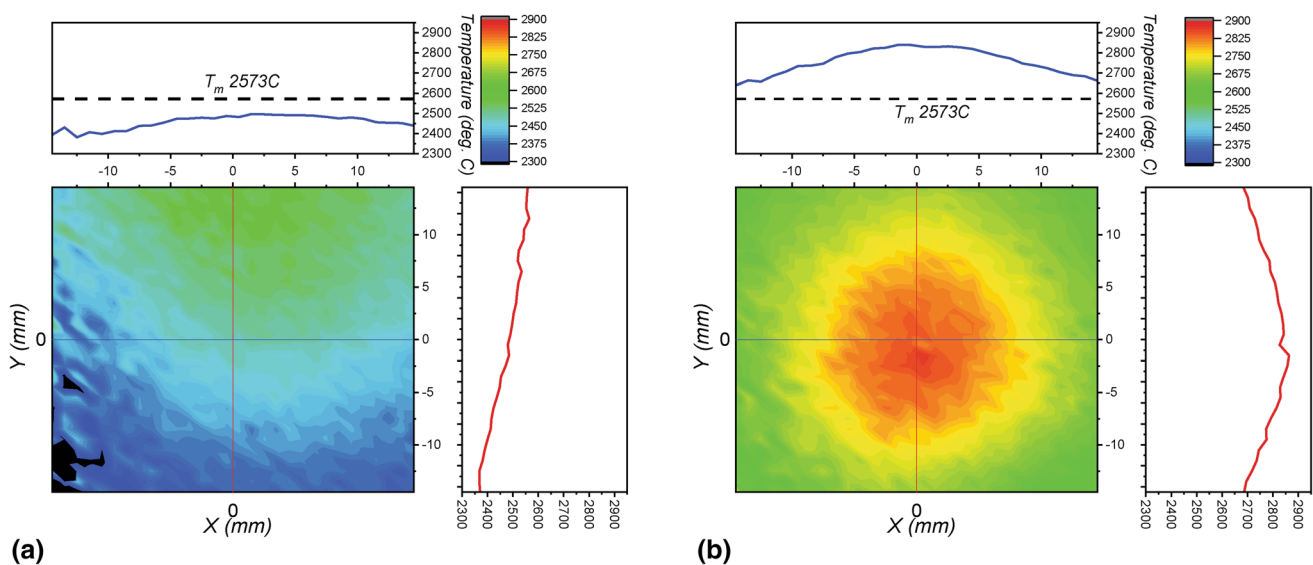


Fig. 7 (a) Thermal mapping in space of the particle temperatures for plasma condition C3 using a conventional plasma spray torch. (b) Particle temperature map in space for the C3 condition using a cascaded arc plasma torch. The scaling on the plots is equivalent

curvature should be much more uniform with this torch configuration than when using a conventional plasma torch.

Figure 8 shows the as-deposited microstructure of a 12.5-mm \emptyset cylinder sprayed with the F4-MB (Sample A3) compared with the microstructure of the TBC produced with the Sinplex-Pro™ torch at the same parameters (Sample A9). The significant differences in porosity are reflected not only in the microstructures shown, but also in the image analysis data, where nearly a 7% reduction in total porosity is observed. This can be owed both to the higher particle temperatures at the time of impact and the melt efficiency of the cascaded plasma gun. Not surprisingly, the cascaded plasma torch also provided much more uniform TBC coatings on 12.5-mm (Sample A9) and 25.4-mm-diameter (Sample A10) cylinders. This data can be seen in Fig. 9 where the as-deposited microstructures for

the two rods are nearly indistinguishable. The image analysis results confirm this, capturing a change in porosity within the standard deviation of the measurement, as seen in Table 2. The data show not only does cascaded plasma torch technology deliver higher particle temperatures, but the uniformity of the thermal field allows the ability to produce microstructural continuity on a variety of surface geometries. Such information provides important considerations for spraying substrate geometries more complex such as turbine blades and vanes.

In this exercise of torch parameter and type, the sensitivity of the particle melt behavior on the final microstructure of a TBC sprayed onto a curved substrate has been observed. From the data, it is clear that by sampling a smaller portion of the plume when spraying curved geometries, the particle melt state at that core has a

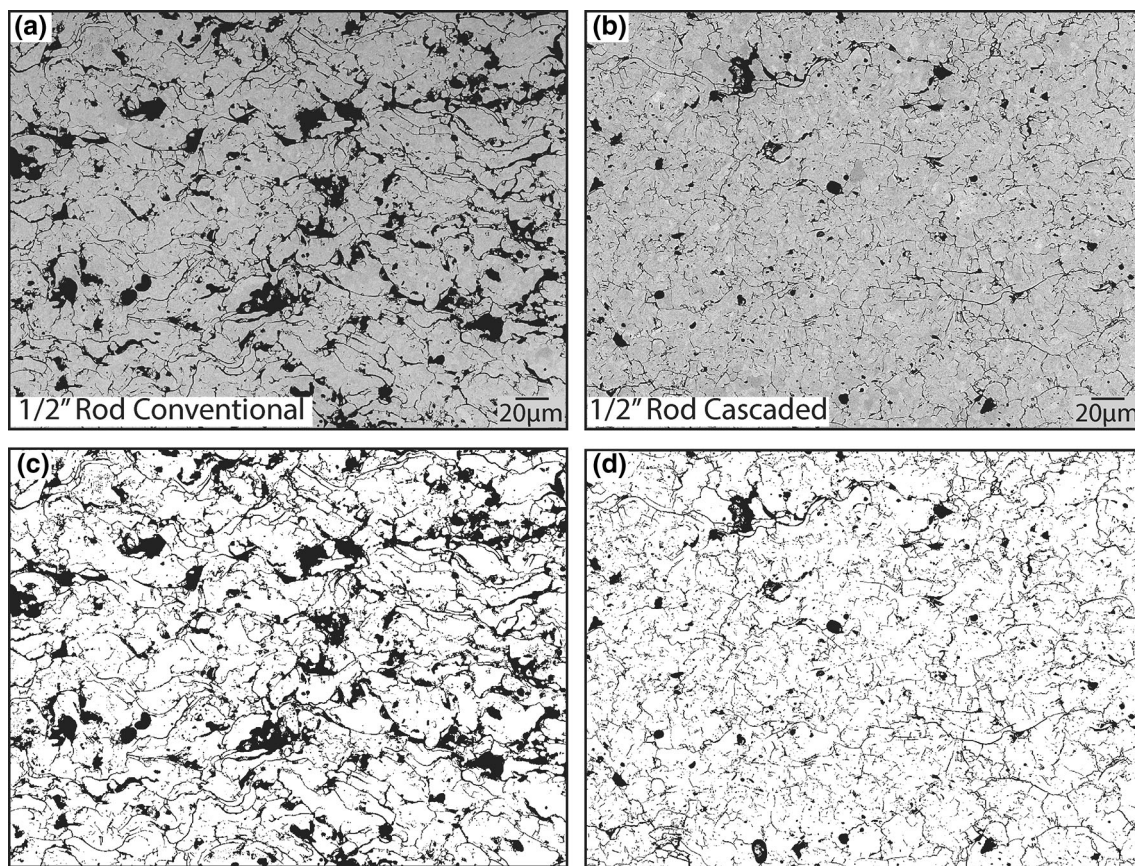


Fig. 8 (a) As-deposited microstructure of a 7YSZ TBC deposited using condition C3 with a conventional torch onto a 12.5-mm \emptyset rod using an ensemble particle size distribution (Sample A3). (b) As-deposited microstructure of a 7YSZ TBC using condition C5 (C3

equivalent) with a cascaded plasma torch deposited onto a 12.5-mm \emptyset rod using an ensemble particle size distribution (Sample A9). (c, d) are the binary thresholded images of (a, b), respectively

significant influence on the intersplat bonding and consequently the overall porosity. To better reflect this behavior, the particle temperature 2-D maps were taken and converted into a melting index parameter. As published originally by Zhang et al. (Ref 35), the melting index is a parameter which can take input parameters such as particle/droplet size, surface temperature, and speed and output a nondimensional parameter. In brief, if the melting index of a particle is at or above zero, it can be considered that droplet at that point in space and time is at the onset of melting. Likewise, a negative melting index suggests the particle is not well-molten, and a positive melting index suggests the particle is increasingly molten as the parameter approaches (and in some cases) exceeds unity. Shown in Fig. 10 are the converted melting index maps. From Fig. 10(a), the periphery of the plume now clearly shows the particles in that region are sub-molten, while those in the center are just above the onset of melting. Thus, the microstructural result of Fig. 3, where a rod which “cuts” the plume through the center produces a denser TBC microstructure, can be directly correlated with these

melting index spatial relationships. Furthermore, to achieve a more porous rod TBC microstructure, the particles not only have to be at lower temperature (Fig. 7a) but evidently have to be semimolten to promote the generation of a porous microstructure, as the melting indices in Fig. 10(b) are all below 0. Finally, to further illustrate the difference of melt efficiency of the cascade torch and its influence on the microstructural generation of TBCs on cylinders, Fig. 10(c) shows even the particles at the periphery have surpassed the onset of melting.

Influence of Outer Diameter of Part on Plasma/Plume/Part Interactions

A tangential study was conducted to attempt to homogenize the microstructures of the 12.5-mm- and 25.4-mm-diameter cylinders by only using the standard plasma torch. Taking into consideration the data from the cascaded torch, an approach toward improving the melt efficiency of the F4-MB was taken. For this, a finer, more uniform particle size distribution of 7YSZ feedstock powder (i.e. 10–50 μm

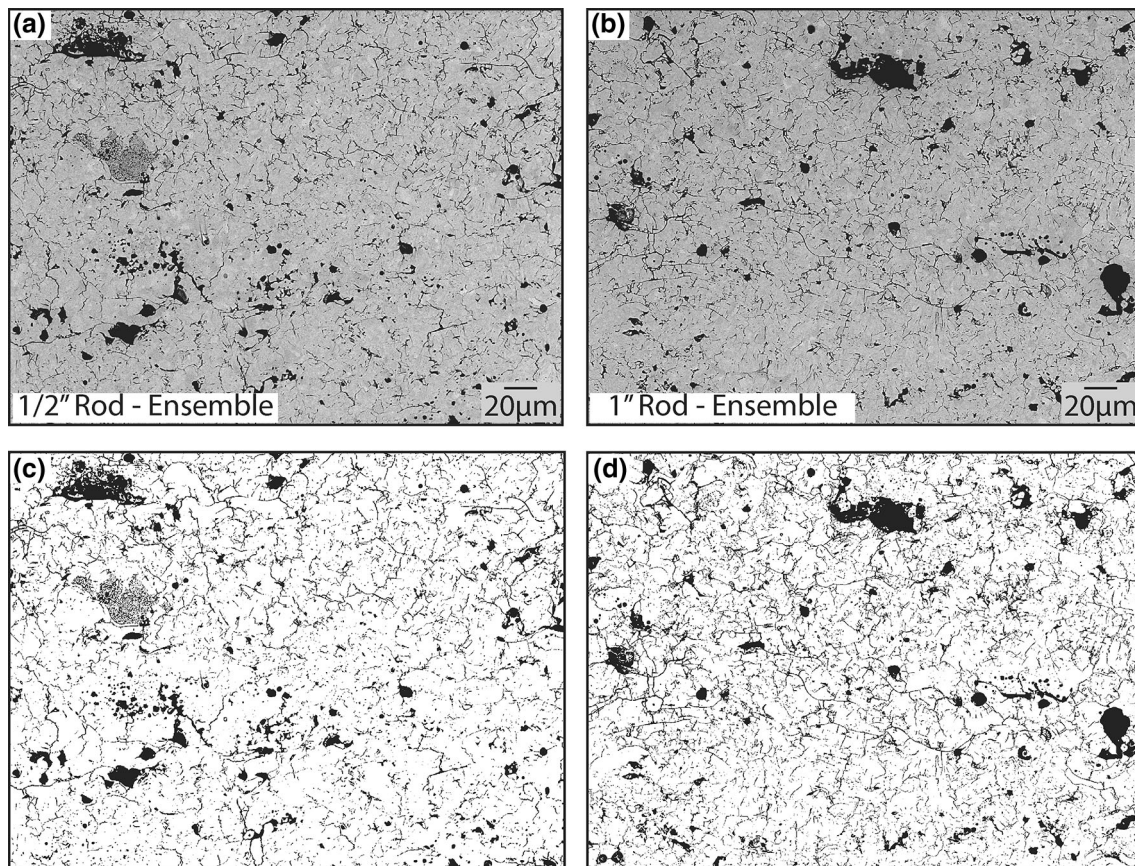


Fig. 9 (a) As-deposited microstructure of a 7YSZ TBC deposited using condition C5 with a cascaded arc plasma torch onto a 12.5-mm \emptyset rod using an ensemble particle size distribution (Sample A9). (b) As-deposited microstructure of a 7YSZ TBC using condition C5

with a cascaded arc plasma torch deposited onto a 25.4-mm \emptyset rod using an ensemble particle size distribution (Sample A10). (c, d) The binary thresholded images of (a, b), respectively

instead of 10–105 μm) was used at the same C3 plasma condition (Sample A7). The resulting as-deposited microstructures from this endeavor can be seen in Fig. 11. Here coatings were again made with the ensemble powder in separate runs from what was previously shown. From the data, it is observed with the ensemble powder there is a discrepancy in the porosity of plasma-sprayed TBCs between the 12.5- and 25.4-mm \emptyset cylindrical substrates. However, with the change in feedstock, this finer, more uniform powder size distribution material has been able to produce microstructures on different rod dimensions which are more similar. This is reflected in the image analysis data shown in Table 2, where the difference in porosity between 12.5- and 25.4-mm-diameter rod TBCs decreased from 4.0 to 2.0% after changing the feedstock (Sample A3 v A4 as compared to Sample A7 v A8, respectively). This suggests the conventional plasma torch also has flexibility in being able to control the microstructure on parts with many complex curved surfaces, albeit through feedstock control. However, as the past literature has shown, simply producing similar microstructures does not mean the

coatings will be the same. Liu et al. and Dwivedi et al. have shown manipulating feedstock while keeping process conditions constant can still have a significant impact on properties such as the stress states in the coatings despite preliminary microstructural similarities (Ref 20, 21, 36). Therefore, it would be beneficial to quantify or characterize what influence the spatial particle state distribution might have on the TBC properties.

Nonlinear Elastic Behavior of Coatings Sprayed at Different Plume Positions

While measurements of porosity by image analysis are indeed useful as a first-order comparison, this study strives to capture as many nuances in the APS deposition process and coating formation dynamics as possible. Figure 12 shows the linear Elastic Modulus vs. Nonlinear Degree for a conventional C3 coating sprayed on a 228.6 mm \times 25.4 mm plate (Sample A5) as opposed to one sprayed on the I-beam geometry sprayed similarly (Sample A6). While the microstructural data do not show

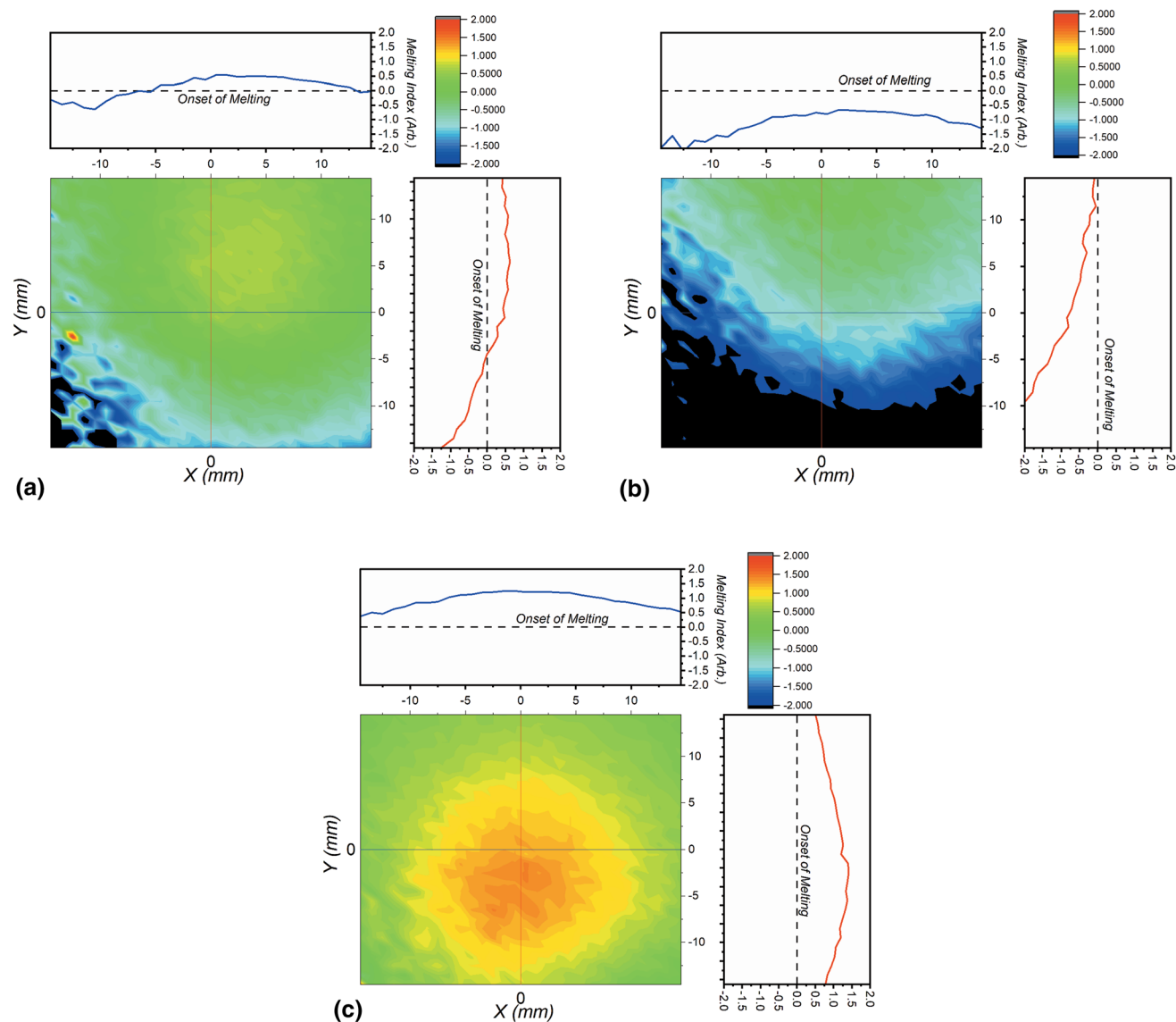


Fig. 10 Converted melting index maps from (a) Fig. 5(a), (b) Fig. 7(a), (c) Fig. 7(b). The 0.0 melting index line is demarcated to illustrate the onset of melting

much evidence suggesting substantial differences, the mechanical property data shown here present these coatings to be much more unique. Even considering as much as a 10% influence/error in measurement on the property data from changing the substrate geometry, differences would still be observable. Therefore, this methodology of “modified beam” curvature techniques allows the ability to quantify on a relative basis how a TBC coated on a sharp edge/curved surface responds to thermal strains as compared to a TBC on a model flat coupon.

Building off the procedure and results from Fig. 12, more permutations of the I-beam experiment were conducted. This time, the effect of plume position as well as particle size distribution was analyzed for the I-beam TBC deposited using the C3 condition. To do so, the coatings

were deposited by rastering the gun back and forth along the surface without stepping vertically (as one would in a ladder deposition pattern). It was found from the measurements that as you go from an off-center spray, where the plume periphery is producing the coating, to a centralized spray, the room-temperature linear elastic modulus of the coating increases. Furthermore, by reducing the particle size distribution of the feedstock, this property can be further altered. This result illustrates the sensitivity of how the coating microstructure develops based on which portion of the plasma plume it is exposed to. Furthermore, it can also be seen while changing the feedstock was able to slightly homogenize the microstructure in a positive way, this does come with the added effect of reducing coating compliance, which may not be desirable (Fig. 13).

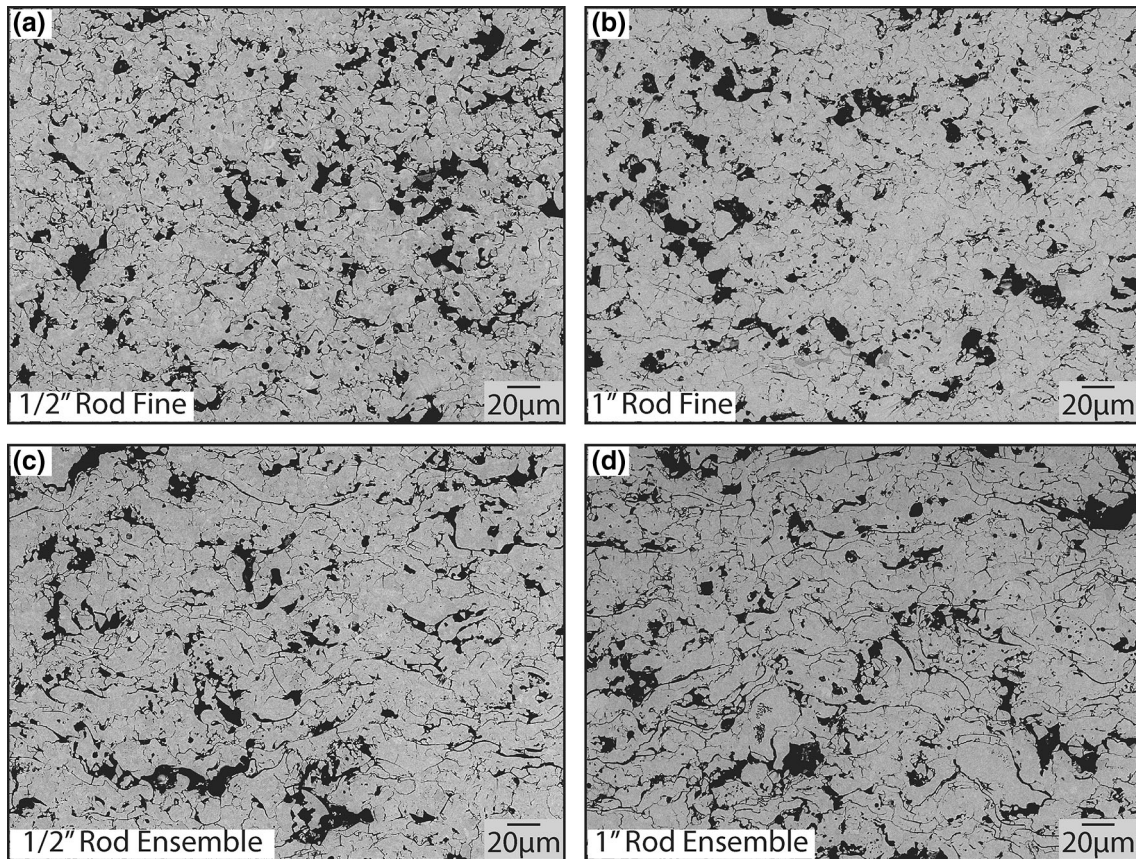


Fig. 11 (a) As-deposited microstructure of a 7YSZ TBC coated rod deposited using condition C3 with a conventional plasma torch and fine particle size distribution on a 12.5-mm \emptyset rod (Sample A7), (b) the same conditions for a 25.4-mm \emptyset rod (Sample A8), (c) as-deposited

microstructure of a 7YSZ TBC-coated rod deposited using condition C3 with a conventional plasma torch and ensemble particle size distribution on 12.5-mm \emptyset rod (Sample A3), (d) the same for a 25.4-mm \emptyset rod (Sample A4)

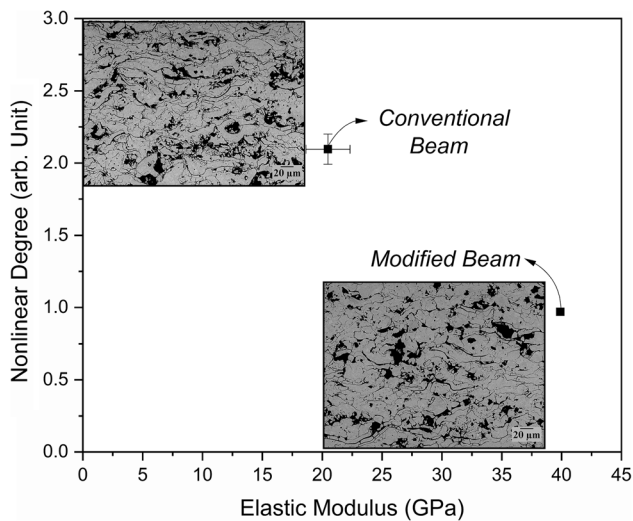


Fig. 12 Measured elastic modulus and nonlinear degree of 7YSZ TBCs deposited using condition C3 on planar surfaces (i.e. Sample A5) and modified geometries (Sample A6) to sample only the center of the plasma plume

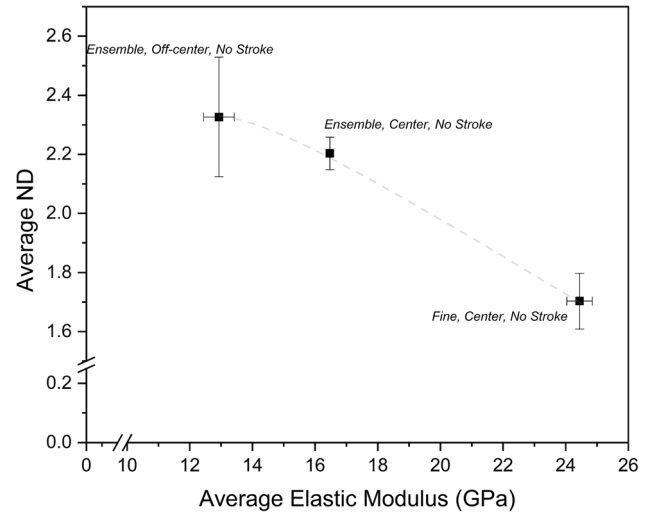


Fig. 13 Measured elastic modulus and nonlinear degree of 7YSZ TBCs deposited using condition C3 on modified geometries to sample only the center of the plasma plume. Particle size distribution and position of the plume with respect to the beam center were manipulated to illustrate the influence of off-angle spraying on TBC microstructure and property

Conclusions

The work presented in this manuscript has shown the influence of the process-induced spatial distribution of particle properties on the resulting microstructure of an air-plasma-sprayed TBC on complex geometries. Through use of particle diagnostic measurements, plasma plume cross-sectional profiles were captured containing information about particle temperature and flow rate as a function of space. These data were then corroborated with microstructural observations of a coating profile as well as different cylinders coated with 7YSZ by the processing methods. The results show the as-deposited microstructure of TBCs sprayed onto cylindrical substrates has a strong dependence on the plume position as well as the overall particle temperature distribution along a given line in space.

It was shown through use of a cascaded plasma torch the thermal profile of the particles could be made more uniform, which in turn allows for the deposition of more uniform coatings on a variety of curved surfaces. Following this realization, an effort was made to improve the thermal efficiency of the conventional plasma torch through use of a finer, more uniformly sized feedstock powder. Doing so proved beneficial to the effort of homogenizing the microstructure between ½” and 25.4-mm \emptyset cylindrical TBCs, as the porosity difference between the two cylinders sprayed with the finer feedstock decreased by nearly 100%. These results were corroborated by taking the spatial plume data and converting it to a spatial melting index map. This map was able to clearly define the origin of porosity of coatings sprayed at or including the plume periphery. In the maps, it was revealed the particles were clearly semimolten or resolidified as their melting indices were significantly below the onset of melting for conventional plasma spray processes.

Finally, to quantify these differences beyond simply porosity measurements by image analysis, a new I-beam substrate geometry was introduced. Here, coatings could be sprayed without using a ladder-step pattern, which allowed sampling portions of the plume in ways similar to how cylinder surfaces/sharp edges would be sprayed. The data suggest there is a potential within this substrate design to be able to probe the influence of plume position, feedstock particle size distribution, and other parameters relevant to spraying on curved surfaces on the resulting mechanical properties of the TBCs. Finally, these analysis techniques have proven to be useful in establishing a robust correlation between processing parameters, the resulting coating microstructure, and the coating properties for spray patterns which mimic what might be done on complex geometries such as a leading edge of a turbine blade.

Acknowledgments This study was supported by the Industrial Consortium for Thermal Spray Technology. We are grateful to Howard Wallar and Tim Vitorino, Saint-Gobain, for providing powders used in this study. The authors thank Oerlikon Metco for support on operation of the Sinplex-Pro™ and the plasma torch hardware.

References

1. S. Sampath, U. Schulz, M.O. Jarligo, and S. Kuroda, Processing Science of Advanced Thermal-Barrier Systems, *MRS Bull.*, 2012, **37**(10), p 903-910
2. A. Feuerstein, J. Knapp, T. Taylor, A. Ashary, A. Bolcavage, and N. Hitchman, Technical and Economical Aspects of Current Thermal Barrier Coating Systems for Gas Turbine Engines by Thermal Spray and EBPVD: A Review, *J. Therm. Spray Technol.*, 2008, **17**(2), p 199-213
3. U. Schulz, B. Saruhan, K. Fritscher, and C. Leyens, Review on Advanced EB-PVD Ceramic Topcoats for TBC Applications, *Int. J. Appl. Ceram. Technol.*, 2004, **1**(4), p 302-315
4. V.K. Tolpygo, D.R. Clarke, and K.S. Murphy, Oxidation-Induced Failure of EB-PVD Thermal Barrier Coatings, *Surf. Coat. Technol.*, 2001, **146-147**, p 124-131
5. D. Liu, C. Rinaldi, and P.E.J. Flewitt, Effect of Substrate Curvature on the Evolution of Microstructure and Residual Stresses in EBPVD-TBC, *J. Eur. Ceram. Soc.*, 2015, **35**(9), p 2563-2575
6. D.D. Hass, A.J. Slifka, and H.N.G. Wadley, Low Thermal Conductivity Vapor Deposited Zirconia Microstructures, *Acta Mater.*, 2001, **49**(6), p 973-983
7. Y.H. Sohn, E.Y. Lee, B.A. Nagaraj, R.R. Biederman, and R.D. Sisson, Microstructural Characterization of Thermal Barrier Coatings on High Pressure Turbine Blades, *Surf. Coat. Technol.*, 2001, **146-147**, p 132-139
8. W.G. Mao, J.P. Jiang, Y.C. Zhou, and C. Lu, Effects of Substrate Curvature Radius, Deposition Temperature and Coating Thickness on the Residual Stress Field of Cylindrical Thermal Barrier Coatings, *Surf. Coat. Technol.*, 2011, **205**(8), p 3093-3102
9. S. Faulhaber, C. Mercer, M.W. Moon, J.W. Hutchinson, and A.G. Evans, Buckling Delamination in Compressed Multilayers on Curved Substrates with Accompanying Ridge Cracks, *J. Mech. Phys. Solids*, 2006, **54**(5), p 1004-1028
10. S. Sampath and H. Herman, Rapid Solidification and Microstructure Development During Plasma Spray Deposition, *J. Therm. Spray Technol.*, 1996, **5**(4), p 445-456
11. X. Jiang, Y. Wan, H. Herman, and S. Sampath, Role of Condensates and Adsorbates on Substrate Surface on Fragmentation of Impinging Molten Droplets During Thermal Spray, *Thin Solid Films*, 2001, **385**(1-2), p 132-141
12. A.T.T. Tran, M.M. Hyland, K. Shinoda, and S. Sampath, Influence of Substrate Surface Conditions on the Deposition and Spreading of Molten Droplets, *Thin Solid Films*, 2011, **519**(8), p 2445-2456
13. S. Sampath and X. Jiang, Splat Formation and Microstructure Development During Plasma Spraying: Deposition Temperature Effects, *Mater. Sci. Eng. A*, 2001, **304-306**, p 144-150
14. H. Zhang, X.Y. Wang, L.L. Zheng, and X.Y. Jiang, Studies of Splat Morphology and Rapid Solidification During Thermal Spraying, *Int. J. Heat Mass Transf.*, 2001, **44**(24), p 4579-4592
15. G. Montavon, S. Sampath, C.C. Berndt, H. Herman, and C. Coddet, Effects of the Spray Angle on Splat Morphology During Thermal Spraying, *Surf. Coat. Technol.*, 1997, **91**(1), p 107-115
16. D. Liu, M. Seraffon, P.E.J. Flewitt, N.J. Simms, J.R. Nicholls, and D.S. Rickerby, Effect of Substrate Curvature on Residual Stresses and Failure Modes of An Air Plasma Sprayed Thermal

- Barrier Coating System, *J. Eur. Ceram. Soc.*, 2013, **33**(15), p 3345-3357
17. M.J. Lance, J.A. Haynes, and B.A. Pint, The Effects of Temperature and Substrate Curvature on TBC Lifetime and Residual Stress in Alumina Scales Beneath APS YSZ, *Surf. Coat. Technol.*, 2016, **308**, p 19-23
 18. J.W. Hutchinson, Delamination of Compressed Films on Curved Substrates, *J. Mech. Phys. Solids*, 2001, **49**(9), p 1847-1864
 19. R.A. Miller and C.E. Lowell, Failure Mechanisms of Thermal Barrier Coatings Exposed to Elevated Temperatures, *Thin Solid Films*, 1982, **95**(3), p 265-273
 20. Y. Liu, T. Nakamura, G. Dwivedi, A. Valarezo, and S. Sampath, Anelastic Behavior of Plasma-Sprayed Zirconia Coatings, *J. Am. Ceram. Soc.*, 2008, **91**(12), p 4036-4043
 21. Y. Liu, T. Nakamura, V. Srinivasan, A. Vaidya, A. Gouldstone, and S. Sampath, Non-linear Elastic Properties of Plasma-Sprayed Zirconia Coatings and Associated Relationships with Processing Conditions, *Acta Mater.*, 2007, **55**(14), p 4667-4678
 22. G. Dwivedi, Y. Tan, V. Viswanathan, and S. Sampath, Process-Property Relationship for Air Plasma-Sprayed Gadolinium Zirconate Coatings, *J. Therm. Spray Technol.*, 2015, **24**(3), p 454-466
 23. S.-H. Leigh and C.C. Berndt, Quantitative Evaluation of Void Distributions within a Plasma-Sprayed Ceramic, *J. Am. Ceram. Soc.*, 2004, **82**(1), p 17-21
 24. P. Gougeon and C. Moreau, In-Flight Particle Surface Temperature Measurement: Influence of the Plasma Light Scattered by the Particles, *J. Therm. Spray Technol.*, 1993, **2**(3), p 229-233
 25. J. Blain, F. Nadeau, L. Pouliot, C. Moreau, P. Gougeon, and L. Leblanc, Integrated Infrared Sensor System for on Line Monitoring of Thermally Sprayed Particles, *Surf. Eng.*, 1997, **13**(5), p 420-424
 26. V. Srinivasan and S. Sampath, Estimation of Molten Content of the Spray Stream from Analysis of Experimental Particle Diagnostics, *J. Therm. Spray Technol.*, 2010, **19**(1), p 476-483
 27. G. Pharr and W. Oliver, Measurement of Thin Film Mechanical Properties Using Nanoindentation, *MRS Bull.*, 1992, **17**(7), p 28-33
 28. C.W. Kang, H.W. Ng, and S.C.M. Yu, Comparative Study of Plasma Spray Flow Fields and Particle Behavior Near to Flat Inclined Substrates, *Plasma Chem. Plasma Process.*, 2006, **26**(2), p 149-175
 29. T. Ba, C.W. Kang, and H.W. Ng, Numerical Study of the Plasma Flow Field and Particle In-flight Behavior with the Obstruction of a Curved Substrate, *J. Therm. Spray Technol.*, 2009, **18**(5), p 858
 30. K. Pourang, Effect of Substrate on In-flight Particle Characteristics in Suspension Plasma Spraying. Masters, Concordia University (2015)
 31. H.-B. Xiong, L.-L. Zheng, and T. Streibl, A Critical Assessment of Particle Temperature Distributions During Plasma Spraying: Numerical Studies for YSZ, *Plasma Chem. Plasma Process.*, 2006, **26**(1), p 53-72
 32. S. Sampath, X.Y. Jiang, J. Matejcek, A.C. Leger, and A. Vardelle, Substrate Temperature Effects on Splat Formation, Microstructure Development and Properties of Plasma Sprayed Coatings Part I: Case Study for Partially Stabilized Zirconia, *Mater. Sci. Eng. A*, 1999, **272**(1), p 181-188
 33. L. Bianchi, A.C. Leger, M. Vardelle, A. Vardelle, and P. Fauchais, Splat Formation and Cooling of Plasma-Sprayed Zirconia, *Thin Solid Films*, 1997, **305**(1), p 35-47
 34. R.C. Seshadri and S. Sampath, Characteristics of Conventional and Cascaded Arc Plasma Spray-Deposited Ceramic Under Standard and High-Throughput Conditions, *J. Therm. Spray Technol.*, 2019, **28**(4), p 690-705
 35. H. Zhang, H.B. Xiong, L.L. Zheng, A. Vaidya, L. Li, S. Sampath, Melting Behavior of In-Flight Particles and Its Effects on Splat Morphology in Plasma Spraying, ed. (2002), p. 309-316
 36. G. Dwivedi, T. Wentz, S. Sampath, and T. Nakamura, Assessing Process and Coating Reliability Through Monitoring of Process and Design Relevant Coating Properties, *J. Therm. Spray Technol.*, 2010, **19**(4), p 695-712

Publisher's Note Springer Nature remains neutral with regard to jurisdictional claims in published maps and institutional affiliations.